ACS OMEGA

http://pubs.acs.org/journal/acsodf

Article

Metallocyclic Cu^{II}–Ln^{III} Single-Molecule Magnets from the Self-Assembly of 1,4-Diformylnaphthalene-2,3-diol

Tyson N. Dais, Rina Takano, Yoshiki Yamaguchi, Takayuki Ishida, and Paul G. Plieger*

Cite This: *ACS Omega* 2022, 7, 5537−5546

Read Online

ACCESS | Metrics & More | Article Recommendations | Supporting Information

ABSTRACT: We report the synthesis and characterization of seven new tetranuclear 3d−4f complexes derived from the 3:3:1 reaction of 1,4-diformylnaphthalene-2,3-diol (H_2**L**) with copper(II) nitrate and a lanthanide salt, Ln = Tb [$L_3Cu_3TbCl_2(NO_3)_2(H_2O)_2$] (**C1**), Ho [$L_3Cu_3HoCl_3(H_2O)_3(MeOH)](H_2O)$ (**C2**), Er [$L_3Cu_3ErCl_3(H_2O)_{3.5}(MeOH)_{0.5}](H_2O)$ (**C3**), Gd [$L_3Cu_3Gd(NO_3)_2(H_2O)_2(MeOH)](NO_3)$ (**C4**), Dy [$L_3Cu_3Dy(NO_3)_2(H_2O)_2(MeOH)](NO_3)$ (**C5**), Yb [$L_3Cu_3Yb(NO_3)_2(H_2O)_2(MeOH)](NO_3)$ (**C6**), and La [$L_3Cu_3La(NO_3)_2(H_2O)_2(MeOH)](NO_3)$ (**C7**). Structural elucidation showed that the self-assembly using the acyclic ligand system was successful for all seven complexes, which exhibit the same near-planar Cu_3LnO_{12} core. Five complexes (**C1**, **C2**, and **C4**−**C6**) were magnetically characterized at 300 K and 1.8 K. Complexes **C1**, **C4**, and **C5** were observed to have ferromagnetic ground states and showed appreciable frequency dependence in their AC magnetic measurements, which yielded effective barriers between 7.82(4) and 13.2(3) K, confirming the presence of single-molecule magnet properties.

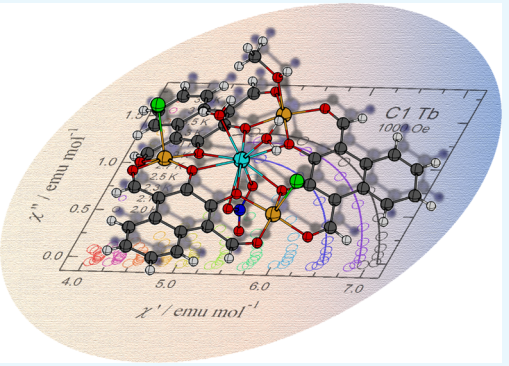

INTRODUCTION

Since the slow relaxation of magnetization in the archetypal Mn_{12} single-molecule magnet (SMM) was first reported nearly three decades ago,[1] the study and application of molecular magnetism have flourished and attracted interest across the fields of chemistry, physics, nanoscience, and materials science.[2−10] At low temperatures, the thermal energy k_BT becomes comparable to the energy barrier for the reversal or relaxation of magnetization, U_{eff}, consistent with a magnetically bistable ground state.[11] A decade after the report of Mn_{12}, the first lanthanide-based SMM was reported, [$LnPc_2$].[12] The heavy rare earth metals have become popular nuclei used to slow or prevent the reversal of magnetization in SMMs due to their large ground-state magnetic anisotropies and spin multiplicities.[13−16] Because of the shielding of 4f electrons in lanthanide ions, the exchange interaction between 4f centers is inherently weak, and thus there has been a focus on combining paramagnetic first row transition metal ions with the lanthanide ions.[17−19] The inclusion of 3d metals in proximity to 4f ions establishes magnetic exchange pathways which can act to suppress the quantum tunnelling of magnetization, a common pitfall of purely 4f SMMs, and increase U_{eff}.[19−21]

A combination of three transition metals and one lanthanide ion have, in the past, been used to template the macrocyclization of 2,3-dihydroxybenzene-1,4-dicarbaldehyde with various diamine linkers.[22−26] The Plieger group have previous experience in preparing multinuclear metal complexes with potentially interesting magnetic properties,[27−30] and the Ishida group have expertise in the magnetic characterization of 3d−4f complexes, particularly those involving copper(II).[31−35] Inspired by the Zn_3La system first reported by Nabeshima et al.[22] and later extended to other metal combinations by Brooker et al.,[24,25,35−40] we investigated the self-assembly and successful crystallization of L_3Cu_3Ln complexes using the acyclic ligand system 1,4-diformylnaphthalene-2,3-diol (H_2**L**). While there are numerous examples of magnetically coupled Cu−Ln systems,[41,42] throughout the literature, there are very few Cu_3Ln complexes featuring four in-plane metal ions;[43−45] and a CCDC search indicated that, outside of the previously mentioned complexes of Nabeshima and Brooker, there are no other structurally characterized examples which exclusively contain Cu−O−Ln bridges. The Brooker group have reported macrocyclic Cu_3Ln complexes for the entire available lanthanide family, excluding promethium. Of the numerous compounds, only variations of the macrocyclic Cu_3Tb complex showed promise as SMMs. Although isolation and structural elucidation of analogous systems prior to Schiff base/macrocycle formation have been reported in the literature,

Received: December 10, 2021
Accepted: January 21, 2022
Published: January 31, 2022

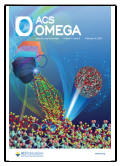

magnetic characterization of such "intermediate" species is notably absent; however, we recently reported the structures and magnetic properties of four acyclic Ni_3Ln complexes containing planar Ni_3LnO_{12} cores.[30] Herein, we extend this to include a series of acyclic Cu_3Ln complexes with near planar Cu_3LnO_{12} cores and report the first magneto−structural correlations for this class of complexes (Figure 1).

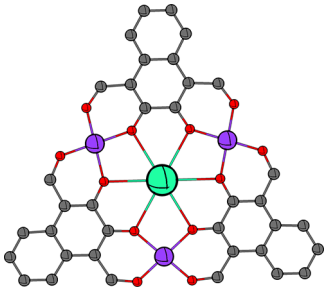

Figure 1. Schematic showing the general metal—ligand connectivity of the complexes reported in this work. Carbon = gray, oxygen = red, Cu^{II} = purple, and Ln^{III} = green.

RESULTS AND DISCUSSION

The addition of a methanolic $Cu(NO_3)_2$ solution (3 equiv.) to the ligand suspension (3 equiv.) was accompanied by rapid dissolution and a subsequent color change from a murky orange-brown to a deep red-brown solution. There were no notable changes upon addition of the lanthanide containing solution (1 equiv) nor were there any changes when the lanthanide metal was added prior to the transition metal solution. IR spectroscopy revealed a new band in the 1610−1616 cm^{-1} region corresponding to the coordinated aldehyde groups, and no bands corresponding to unreacted aldehyde (1673 and 1641 cm^{-1}) were present. X-ray quality single crystals of **C1**−**C7** were grown by vapor deposition of diethyl ether into a concentrated methanolic solution of the complex. Two complexes (**C2** and **C3**) crystallized in the orthorhombic space group *Pbcn*, and the other five complexes crystallized in the monoclinic space groups (**C1** in $P2_1$, and the remaining five complexes in $C2/c$), with $\pi-\pi$ stacking being the dominant supramolecular interaction in all seven complexes. Selected bond lengths and angles are given in Table 1 as ranges over all copper ions in each complex. Crystal packing diagrams and details on interactions can be found in Supporting Information, Figures S1−S8. Bulk purity was confirmed by microanalytical analysis. Continuous shape measurement (CShM) calculations[46,47] indicate that all copper ions have approximately *C*4v square pyramidal geometries (average CShM values for SPY-5 geometry: **C1** 1.01, **C2** 1.08, **C3** 1.07, **C4** 0.646, **C5** 0.649, **C6** 0.771, and **C7** 0.689). CShM values below unity correspond to complexes which crystallize in the monoclinic space group $C2/c$. The geometry of Cu4 in each complex also tends toward *C*4v vacant octahedron geometry (**C1** 1.13, **C2** 1.34, **C3** 1.33, **C4** 1.07, **C5** 1.22, **C6** 1.48, and **C7** 1.26).

The crystal structure of **C1** (Figure 2) revealed a relatively nonplanar system with a mixture of nitrate and chloride caps. Although **C1** was not the only complex prepared using a $LnCl_3{\cdot}xH_2O/Cu(NO_3)_2{\cdot}3H_2O$ combination, it is the only complex to feature both chloride and nitrate capping groups—as confirmed by single-crystal X-ray diffraction and elemental

Table 1. Selected Structural Parameters for C1−C7

Distance/Å	C1	C2	C3	C4	C5	C6	C7
$Ln^{III}-O_{phenol}$	2.415(12)−2.531(12)	2.420(3)−2.463(3)	2.410(3)−2.462(3)	2.488(8)−2.524(6)	2.458(7)−2.517(8)	2.435(6)−2.513(6)	2.477(8)−2.524(8)
$Ln^{III}-O_{nitrate}$	2.434(20)−2.532(18)			2.415(14)−2.488(15)	2.395(13)−2.456(12)	2.305(13)−2.395(14)	2.367(10)−2.444(12)
$Ln^{III}-O_{water}$	2.389(15)−2.513(18)	2.298(3)−2.374(3)	2.276(4)−2.362(4)				
$Cu^{II}-O_{phenol}$	1.900(15)−1.935(14)	1.909(3)−1.941(3)	1.906(4)−1.948(3)	1.883(7)−1.914(8)	1.880(8)−1.907(9)	1.843(7)−1.900(8)	1.865(7)−1.921(8)
$Cu^{II}-O_{formyl}$	1.898(19)−2.014(15)	1.916(3)−1.978(3)	1.916(3)−1.978(4)	1.884(9)−1.950(9)	1.902(10)−1.930(9)	1.880(9)−1.946(9)	1.904(9)−1.946(9)
$Cu^{II}-O_{water}$			2.368(9)	2.259(16)−2.320(20)	2.246(14)−2.273(17)	2.207(17)−2.230(20)	2.283(13)−2.302(15)
$Cu^{II}-O_{methanol}$	2.212(19)	2.371(4)	2.368(9)[a]	2.220(20)	2.270(20)	2.378(18)	2.287(18)
$Cu^{II}-Cl$	2.502(7)−2.578(8)	2.478(1)−2.532(1)	2.473(2)−2.530(2)				
Av. $Cu^{II}\cdots Cu^{II}$	6.162(4)	6.113(1)	6.111(1)	6.225(3)	6.215(3)	6.182(3)	6.211(3)
Av. $Cu^{II}\cdots Ln^{III}$	3.562(4)	3.538(1)	3.537(1)	3.594(2)	3.589(2)	3.570(2)	3.586(2)
Min. $Ln^{III}\cdots Ln^{III}$	9.988(2)	9.757(1)	9.752(1)	9.668(1)	9.710(1)	9.741(1)	9.675(1)
Angle/°							
$Cu^{II}-O-Ln^{III}$	108.3(6)−111.2(7)	106.9(1)−108.3(1)	107.1(2)−108.6(2)	107.4(4)−109.1(4)	107.6(4)−109.5(3)	107.5(3)−110.6(4)	107.4(3)−109.8(3)

[a]Crystallographically disordered H_2O/MeOH cap with the oxygen atom occupying the same coordinate.

https://doi.org/10.1021/acsomega.1c07001
ACS Omega 2022, 7, 5537−5546

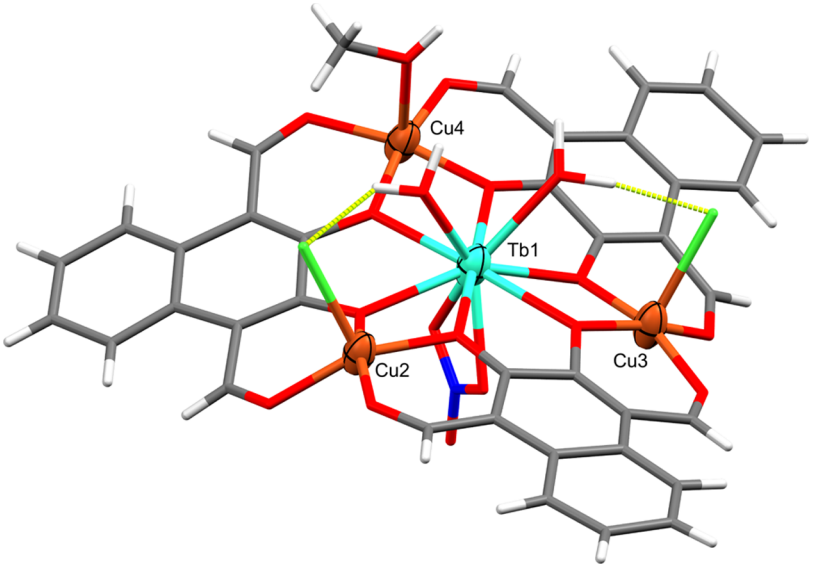

Figure 2. X-ray crystal structure of **C1**. Thermal ellipsoids of metal atoms shown at 50% probability. Carbon = gray, oxygen = red, nitrogen = blue, and chlorine = green. Hydrogen bonds shown as a segmented yellow bond.

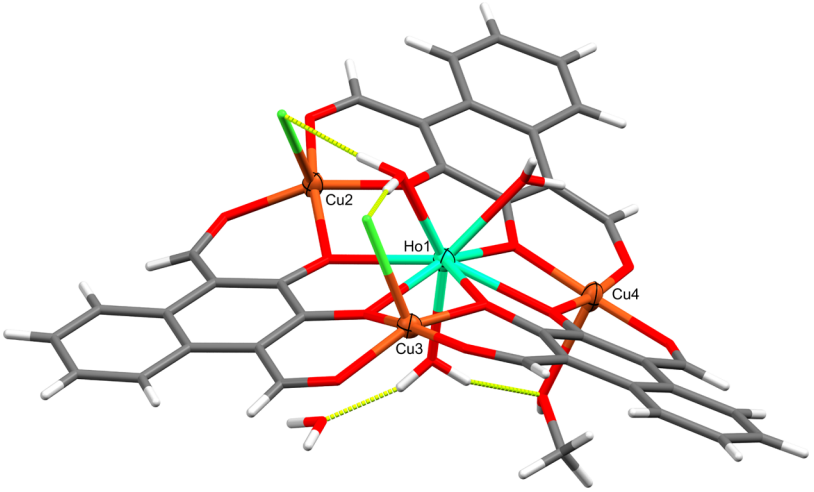

Figure 3. X-ray crystal structure of **C2**. Thermal ellipsoids of metal atoms shown at 50% probability. Carbon = gray, oxygen = red, nitrogen = blue, and chlorine = green. Hydrogen bonds shown as a segmented yellow bond.

analyses. As expected, the large Tb^{III} sits in the middle of an O_6 equatorial binding environment formed from the three sets of catechol-like groups with its axial sites occupied by two water molecules on one side of the Cu_3 plane and a η_2-NO_3 group on the other side of the plane. Each Cu^{II} sits in a square pyramidal coordination environment bound between a phenol and an aldehyde each from two ligand units. In the case of **C1**, the copper ions are axially capped by either a chloride (Cu2 and Cu3) or a methanol molecule (Cu4), with all three copper ions being capped on the same side of the Cu_3 plane. While the entire ligand unit that bridges Cu2 and Cu4 sits below the Cu_3 plane, the remaining two ligand units form a separate plane, and the terbium ion is displaced above the Cu_3 plane by 0.162(3) Å.

The two complexes which crystallized in the orthorhombic space group *Pbcn*, **C2** (Figure 3) and **C3**, are isomorphous and feature only chloride capping groups. The Ln^{III} center in each of these complexes is displaced above the Cu_3 plane by 0.245(1) Å, with the ligand unit bridging Cu2 and Cu3 in each sitting well below the plane. Much like **C1**, Cu2 and Cu3 are each axially capped by a chloride on one side of the plane, while Cu4 is axially capped below the Cu_3 plane. The Cu4 cap is the only structural difference between **C2** and **C3**, with the Cu4 cap of **C2** being a methanol molecule, whereas for **C3**, it was crystallographically determined as a disordered one-to-one mixture of water and methanol. Holmium and erbium, being slightly smaller than terbium, occupy nine-coordinate sites in **C2** and **C3** each with two water caps above the plane and one below. In **C1**, the Cu−Cl bonds can be thought of as diverging away from the catechol moiety which bridges Cu2 and Cu3 (forming a 129.6° angle from the centroid of the two oxygen atoms, O2 and O3) allowing for a parallel arrangement of water caps on Tb1 with a Cl−Cl separation of 8.327 Å. This allows the chloride caps to each accept a hydrogen bond from a different water molecule (O14−H14A···Cl1 = 2.494 Å and O15−H15A···Cl2 = 2.047 Å). In contrast, the Cu−Cl bonds in **C2** and **C3** converge relative to their respective catechol O2−O3 centroid (forming 77.1 and 76.9° angles, respectively). The much smaller Cl−Cl separations (4.828 Å for **C2** and 4.914 Å for **C3**) means the two water caps on Ho1 and Er1 run

https://doi.org/10.1021/acsomega.1c07001
ACS Omega 2022, 7, 5537−5546

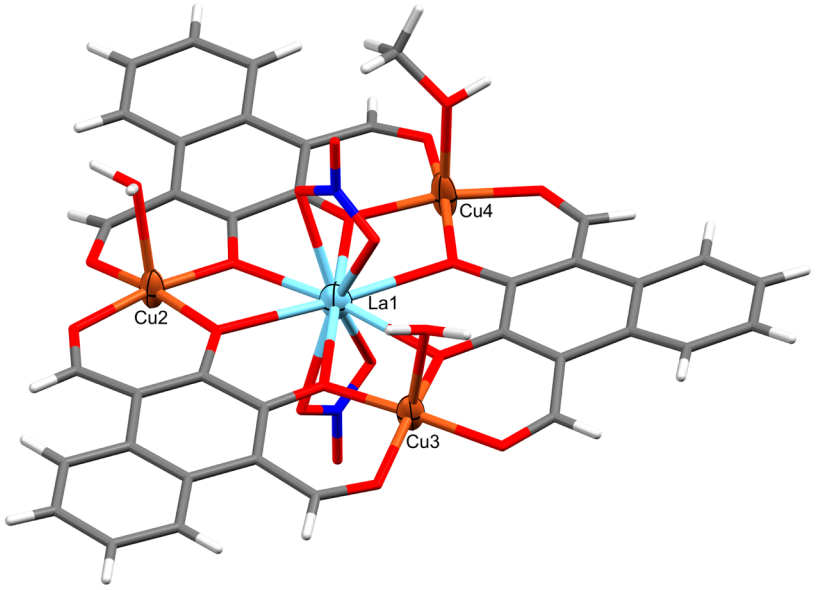

Figure 4. X-ray crystal structure of **C7**. Thermal ellipsoids of metal atoms shown at 50% probability. Carbon = gray, oxygen = red, and nitrogen = blue.

Table 2. Magnetic Properties of C1, C2, C4, C5, and C6

Complex	g_J of Ln^{III}	$\chi_m T$/cm^3 K mol^{-1} (exp. at 300 K)[a]	$\chi_m T$/cm^3 K mol^{-1} (calculated)	$M/N_A\mu_B$ (exp. at 7 T)[b]	$M_{sat}/N_A\mu_B$ (calculated)
C1	3/2	11.70	12.9	7.52	12[c]
C2	5/4	13.79	15.2	7.81	13[c]
C4	2	9.06	9.00	9.84	10
C5	4/3	14.06	15.3	7.98	13[c]
C6	8/7	3.63	4.39	4.39	7[c]

[a]Measured at 500 Oe, fixed with eicosane. [b]Measured at 1.8 K, fixed with eicosane. [c]Calculated for strongly anisotropic Ln^{III} ions where $|J_z| \approx J$.

perpendicular with a single water molecule forming hydrogen bonds to both Cl1 and Cl2 (average of 2.029 Å for **C2** and 2.122 Å for **C3**). Considering the charge balance of the elements present in the crystal structure, an additional negative charge is required per unit complex. A third, non-coordinated chloride anion was crystallographically observed in both **C2** and **C3** but was heavily disordered over multiple sites which were not stable to refinement, and has thus been included within identical solvent masks for each complex of 38 electrons in 98 Å^3 which is consistent with the presence of one chloride and two water molecules per unit complex. This final charge being present as a chloride rather than a nitrate (as in **C1**) is also consistent with the nitrogen content determined by elemental analyses.

Complexes **C4**, **C5**, **C6**, and **C7** (Figure 4) are isomorphous and crystallize in the monoclinic space group *C*2/*c*. They form relatively planar complexes with only minor deviations of the Ln^{III} center and ligands from the Cu_3 plane. Each Ln^{III} center is 10-coordinate with an axially bound η_2-NO_3 group on both sides of the Cu_3 plane, with the Cu^{II} centers of each complex being square pyramidal and all bound on the same side of the Cu_3 plane. Gd1 is displaced below the Cu_3 plane by 0.050(2) Å, while Dy1 and La1 are each displaced below their respective Cu_3 plane by 0.053(2) Å and Yb1 is displaced below its Cu_3 plane by 0.060(2) Å. Each complex contains two water caps (on Cu2 and Cu3) and a methanol cap (on Cu4), with the axial sites of each copper in **C6** being poorly ordered and modeled with only 50% chemical occupancy. All four of these complexes exhibited further crystallographic disorder with the location of a non-coordinated nitrate which is required to balance all charges. This nitrate group was identified to occupy a special position on a 2-fold rotation axis in **C4**, **C5**, and **C6**, with 50% occupancy per unit complex. For **C4**, a disordered fragment of a nitrate anion was located but was only stable to refinement at 25% occupancy, with the remaining 25% occupancy being contained within a solvent mask. In **C5**, the remaining half occupancy nitrate was located and stable to refinement only when very hard isotropic restraints were applied. The remaining half occupancy nitrate for **C6** and the one nitrate per unit complex for **C7** could not be located via the difference map and thus were included in a solvent mask. The formulation of these complexes to include the non-coordinated nitrates within a solvent mask is consistent with elemental analyses.

Magnetic Analysis. Five of the complexes reported here (**C1**, **C2**, **C4**, **C5**, and **C6**) have been magnetically characterized (Table 2). The other two complexes, **C3** and **C7**, could not be prepared in sufficient quantities to facilitate magnetic characterization.

DC Magnetic Measurements. It was found that upon decreasing the temperature, **C2** and **C6** both exhibited a monotonic decrease in the $\chi_m T$ product (Figure 5a) which may be associated with the progressive depopulation of the Stark sublevels of each lanthanide ion. This suggests an apparent weak antiferromagnetic coupling between the Cu^{II} and Ln^{III} ions, which is further evidenced by the $M - H$ data collected (*vide infra*).

https://doi.org/10.1021/acsomega.1c07001
ACS Omega 2022, 7, 5537−5546

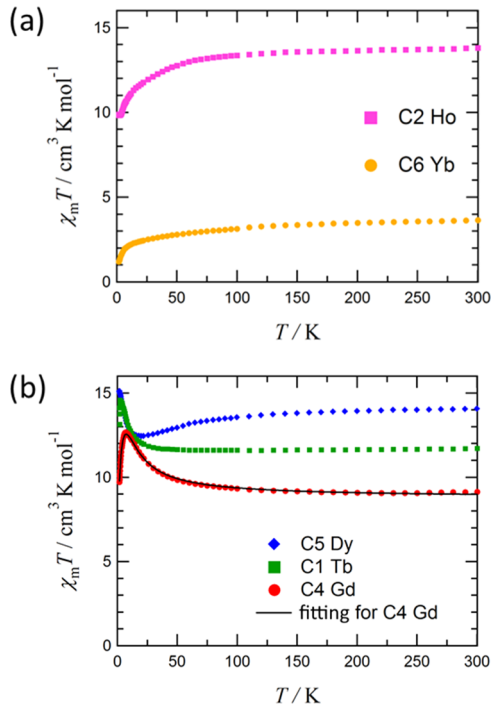

Figure 5. Plots of $\chi_m T$ vs T for (a) **C2** and **C6** and (b) **C1**, **C4**, and **C5** measured at 500 Oe below 100 K and at 5000 Oe above 100 K.

Complexes **C1**, **C4**, and **C5** all exhibited a sharp increase in the $\chi_m T$ product when cooled below ca. 50 K, with **C1** reaching a peak of 14.6 cm^3 K mol^{-1} at 2.2 K and **C4** reaching a peak of 12.5 cm^3 K mol^{-1} at 7.5 K (Figure 5b). These peaks strongly suggest ferromagnetic coupling between the Ln^{III} and Cu^{II} centers. The M vs H measurement for **C4** (Figure 6) unequivocally evidences a high-spin ground state of S_{total} = 10/2. The $\chi_m T$ vs T plot for **C4** shows a monotonic increase down to 7.5 K originating from the three Cu^{II}–Gd^{III} interactions. Quantitative separation of J-coupling terms is difficult due to the approximate C_{3h} symmetry about the Gd^{III} center of **C4**, and thus to avoid overparameterization, **C4** has been approximated to feature only a single Cu–Gd^{III} coupling term, that is, $J_{12} = J_{13} = J_{14} = J$, where J can be estimated with the following van Vleck equation (eq 1) based on the spin Hamiltonian $\boldsymbol{H} = -2J(\boldsymbol{S}_1\cdot\boldsymbol{S}_2 + \boldsymbol{S}_1\cdot\boldsymbol{S}_3 + \boldsymbol{S}_1\cdot\boldsymbol{S}_4)$

$$\chi_m T = \frac{2N_A^2 g_{ave}^2 \mu_B^2}{k_B} \frac{T}{T-\theta} \frac{A}{B} \quad (1)$$

where

$$A = 5\exp(-24J/k_B) + 14\exp(-18J/k_B) + 28\exp(-15J/k_B) + 30\exp(-10J/k_B) + 60\exp(-7J/k_B) + 55$$

$$B = 5\exp(-24J/k_B) + 7\exp(-18J/k_B) + 14\exp(-15J/k_B) + 9\exp(-10J/k_B) + 18\exp(-7J/k_B) + 11$$

The Weiss mean field parameter, θ, has also been included to account for intermolecular interactions. Optimization of eq 1 gave $2J/k_B$ = +5.78(6) K, g_{ave} = 1.976(2), and θ = −0.898(7) K. The calculated curve reproduced the trend of the experimental data well (Figures 5b and 6b). The final $\chi_m T$ drop below 7 K could not be reproduced when modeling the Cu–Cu interactions (J_{23}, J_{24}, and J_{34}; see Figure S9 in the Supporting Information) with MAGPACK.[48,49]

Figure 6 shows the magnetization curves for fixed polycrystalline samples of **C1**, **C2**, **C4**, **C5**, and **C6**, as

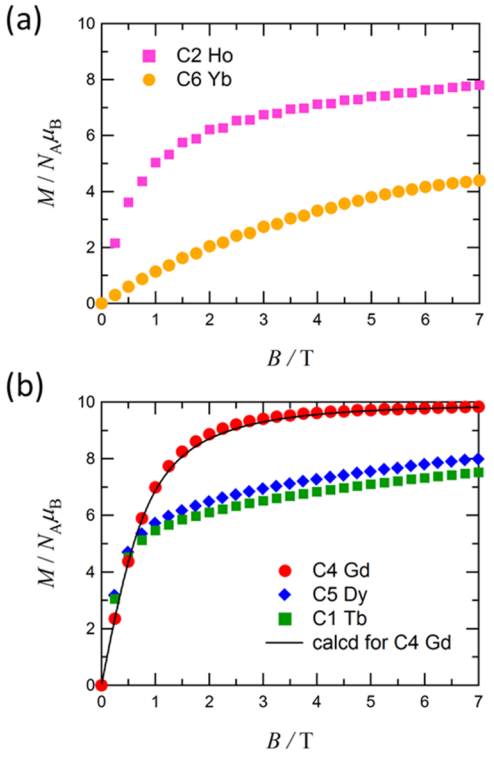

Figure 6. Magnetization plots for (a) **C2** and **C6** and (b) **C1**, **C4**, and **C5** (b) measured at 1.8 K.

measured at 1.8 K. The magnetization of **C4** exhibited the theoretical saturation magnetization (M_{sat}) with 10 $N_A\mu_B$, and those of **C1** and **C5** did not reach the theoretical M_{sat} values at 7 T (Table 2) owing to the presence of strong magnetic anisotropy. However, these values exceeded the antiferromagnetic limit values, thus supporting the presence of a ferromagnetic ground state. The magnetizations of **C2** and **C6** similarly exceeded the antiferromagnetic limit, but practically noncoupled systems would also show similar behavior due to the additive property. Combining the susceptibility results, we can cautiously conclude that the Ho–Cu and Tb–Cu exchange couplings in **C2** and **C6**, respectively, are weak.

AC Magnetic Measurements. As expected from the DC measurements, only **C1**, **C4**, and **C5** exhibited meaningful frequency dependence for the AC susceptibility measurements (Figure 7 for **C1** and Figure S10, Supporting Information for **C1**, **C4**, and **C5**). Complex **C1** exhibited slow relaxation of magnetization as indicated by the appreciable frequency dependence of the AC susceptibility below ca. 5 K (Figure 7). The effective barrier to the reversal of magnetization, U_{eff}, for **C1** was estimated using a modified Arrhenius plot (Figure 8a) according to eq 2[50]

$$\ln\left(\frac{\chi''}{\chi'}\right) = \ln(2\pi\nu\tau_0) + \frac{U_{eff}}{k_B T} \quad (2)$$

https://doi.org/10.1021/acsomega.1c07001
ACS Omega 2022, 7, 5537−5546

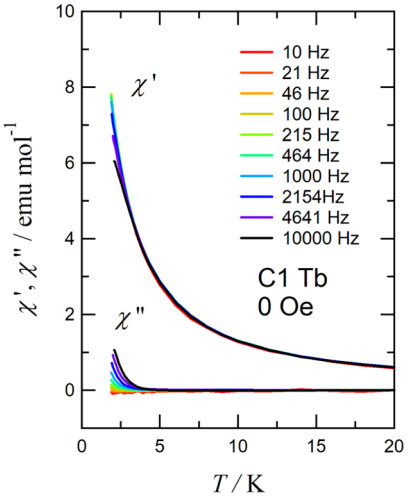

Figure 7. Temperature and frequency dependence of the AC susceptibilities in the zero applied DC field.

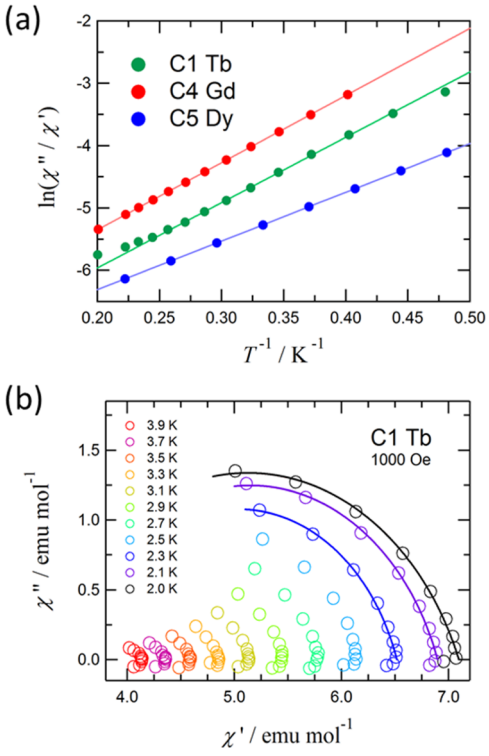

Figure 8. (a) Modified Arrhenius plots for the 1000 Hz data of **C1** in the zero applied DC field, **C4** in a 2000 Oe static field, and **C5** in a 1000 Oe static field. (b) Cole−Cole plot for **C1** with traces for data sets recorded at 2.0, 2.1, and 2.3 K.

The U_{eff} values are 10.49(8) K (zero applied bias) and 13.3(2) K (1000 Oe applied bias; Figure S11a, Supporting Information), with τ_0 values of 5.02×10^{-8} and 3.1×10^{-8} s, respectively. Similarly, **C4** and **C5** showed appreciable frequency-dependent AC susceptibilities below 5 K with applied DC bias fields of 2000 and 1000 Oe, respectively. As Figure 8a shows, optimization of eq 2 for **C4** and **C5** leads to U_{eff} values of 10.8(2) and 7.82(4) K and τ_0 values of 8.8×10^{-8} and 6.05×10^{-8} s, respectively. Details on various DC bias fields are shown in Figure S11, Supporting Information.

Figure 8b shows the Cole−Cole plot for **C1** in the presence of 1000 Oe static magnetic field at the indicated temperatures. The solid line represents the best fit obtained at the given temperature by considering the generalized Debye model[51]

$$\chi(\omega) = \chi_S + \frac{(\chi_T - \chi_S)}{1 + (i\omega\tau)^{1-\alpha}} \quad (3)$$

where χ_S is the adiabatic susceptibility, χ_T is the isothermal susceptibility, ω is the frequency, τ is the relaxation time, and α is the Cole−Cole parameter.[52] The best fit lines at 2.0, 2.1, and 2.3 K almost trace quarter circles where α = 0.24(2), 0.21(2), and 0.19(5), respectively. In this low-temperature regime, the thermal energy is of the order of the exchange-coupled excited states, thus allowing thermal population of these states and serving as a magnetization relaxation pathway, where the Orbach process may be operative. Unfortunately, a normal Arrhenius plot cannot be drawn from the data, so the operative relaxation mechanisms cannot be determined with accuracy; however, the relatively small Cole−Cole parameter values indicate that only a single relaxation process is likely to be occurring.

Table 3 summarizes the results of the AC magnetic susceptibility measurements. In general, superexchange between the $3d_{x^2-y^2}$ and $4f$ spins of heavy lanthanide metals depends on the geometry of the Cu−O−Ln−O four-membered chelate ring, where more planar MO_2 and LnO_2 dihedral angles will lead to stronger ferromagnetic coupling.[53−56] Based on the *macrocyclic* Cu_3Ln analogues previously prepared by Brooker et al., **C1**, containing the Cu_3TbO_6 core, was expected to show the greatest potential as an SMM with the $Cu_3Tb\mathbf{L}^{Bu}$ complex[57] ($\mathbf{L}^{Bu}$ = 3 + 3 Schiff base of 1,4-diaminobutane and 1,4-diformyl-2,3-dihydroxybenzene) containing a 10-coordinate Tb ion reported to have a barrier of 19.5(5) K. A smaller $Cu_3Tb\mathbf{L}^{Pr}$ analogue[24] ($\mathbf{L}^{Pr}$ = 3 + 3 Schiff base of 1,3-diaminopropane and 1,4-diformyl-2,3-dihydroxybenzene), which contained a nine-coordinate Tb ion, was also determined to be an SMM although a barrier height could not be extracted. **C1**, being a Kramers-type molecule, indeed shows the most promising SMM properties as indicated by the magnitude of χ' and its frequency dependence. **C4** and **C5** also showed appreciable frequency dependence in an applied field but yielded lower effective barriers, which may be related to the fact they are not Kramers-type molecules.[32,58] Since Gd^{III} itself is an isotropic ion, the origin of the slow relaxation of magnetization for **C4** is unclear; however, the observed anisotropy could arise from an asymmetric crystal field environment where J_z is not equal to J_x and J_y.[59]

Table 3. Summary of the AC Susceptibility Measurements

Complex	H/Oe	$\tau_0/10^{-8}$ s	U_{eff}/k_B K
C1	0	5.02(14)	10.49(8)
	1000	3.1(2)	13.3(2)
	2000	3.6(3)	13.2(3)
C4	2000	8.8(6)	10.8(2)
C5	1000	6.05(11)	7.82(4)

CONCLUSIONS

The reaction between the ligand, $H_2\mathbf{L}$, and $Cu(NO_3)\cdot 3H_2O$ with various lanthanide salts has yielded seven new complexes which have been characterized by single-crystal X-ray diffraction. These self-assembled metallo−cyclic complexes had previously been overlooked in favor of macrocyclic

https://doi.org/10.1021/acsomega.1c07001
ACS Omega 2022, 7, 5537−5546

analogues where peripheral diimine chelators are typically used to stabilize complexes involving a transition metal ion with five- or six-membered chelation rings. Macrocyclic ligand formation was found to be unnecessary in the construction of the self-assembled tetranuclear clusters in the present system. The compartmental ligand in this work being acyclic in nature is in sharp contrast to the work by Nabeshima et al.[8] Complexes **C2** and **C3** were both prepared using $LnCl_3{\cdot}6H_2O$ salts [Ln = Ho (**C2**) and Er (**C3**)] and were found to be isomorphous containing only the chloride ions present from the lanthanide salt. Similarly, complexes **C4**−**C7** are all isomorphous in the monoclinic space group *C*2/*c*, containing only nitrate ions despite the presence of the acetate from $Yb(OAc)_3{\cdot}6H_2O$ in the preparation of **C6**. Five of the complexes (**C1**, **C2**, and **C4**−**C6**) were prepared in sufficient quantity and purity to elicit magnetic characterization. DC susceptibility measurements implied a ferromagnetic ground state in three of the complexes (**C1**, **C4**, and **C5**). Furthermore, the three compounds exhibited appreciable frequency dependence in their AC magnetic measurements. Macrocyclic analogues indicated that the Tb^{III}-centered complex was likely to exhibit SMM properties; however, observation of the slow relaxation of magnetization in monomeric Cu_3Ln (Ln = Gd or Dy) complexes of this type had yet to be reported. Fitting of the AC data yielded small values of the Cole−Cole parameter, α, implying that only a single relaxation pathway is present for the three SMM candidates. Complex **C1**, containing Tb^{III}, is a Kramers-type molecule and had an observable barrier to relaxation even with zero applied bias, with the maximum barrier determined to be 13.3(2) K in a 1000 Oe applied field. Complexes **C4** and **C5** are not Kramers-type molecules but still yielded meaningful frequency dependence in their AC susceptibility measurements. The Gd-containing complex, **C4**, was found to have a barrier to relaxation of 10.8(2) K in a 2000 Oe applied bias, while **C5**, the Dy containing complex, had a barrier energy of only 7.82(4) K in a 1000 Oe applied bias. Observation of the slow relaxation of magnetization in this type of Cu_3Ln complex which utilizes an acyclic ligand system has not yet been reported in the literature. Investigation of analogous systems using 3d metals with a greater number of unpaired electrons such as $Mn^{II/III}$, Fe^{III}, or Co^{III} could yield even more promising results.

EXPERIMENTAL SECTION

General Experimental Section. All experiments were carried out in air. Solvents and reagents were used as received from commercial sources (Merck/Sigma-Aldrich, Thermo-Fisher) without further purification. The synthesis of ligand H_2**L** has recently been reported[30] and was adapted from the method originally reported by MacLachlan et al.[60] IR spectra were collected on a Nicolet 5700 FT-IR spectrometer with an ATR sampling accessory. Elemental analyses were determined by the Campbell Microanalytical Laboratory at the University of Otago.

Single-crystal X-ray diffraction experiments were carried out on a Bruker D8 Venture diffractometer equipped with an IμS Diamond microfocus Cu K_α source (λ = 1.54187 Å) and a Photon III detector. Single crystals were mounted on MiTeGen mylar loops using Fomblin Y perfluoroether oil and cooled to 100 K with an Oxford Cryostream 800. Data were collected and processed using the APEX3 software package.[61] The structures were solved by intrinsic phasing with SHELXT[62] and refined against least-squares using SHELXL[63] as implemented in Olex2.[64] Non-hydrogen atoms were refined anisotropically, and hydrogen atoms were calculated to their ideal positions unless otherwise stated and refined using a riding model with fixed U_{iso} values. Crystal structure and refinement details for **C1**−**C7** can be found in Table S1, Supporting Information. CCDC deposition numbers 2103942−2103948.

Magnetization and magnetic susceptibility measurements were carried out with a Quantum Design MPMS-XL7 SQUID magnetometer using a static field of 0.05 T. A field of 0.5 T was used to measure the susceptibility of samples with small magnetic moments. Measurements were corrected with diamagnetic blank data from the empty sample holder. The diamagnetic contribution of the sample itself was estimated using Pascal's constants. The AC magnetic susceptibilities were recorded on a Quantum Design PPMS apparatus equipped with an AC/DC magnetic susceptibility option. To avoid possible field-alignment effect, the polycrystalline samples were fixed with a small amount of eicosane.

General Procedure for the Preparation of Complexes C1−C7. $Cu(NO_3)_2{\cdot}3H_2O$ (121 mg, 0.5 mmol) was reacted with H_2**L** (108 mg, 0.5 mmol) and the corresponding lanthanide salt (0.167 mmol) in methanol (10 mL) in a 3:3:1 equiv. Each mixture was stirred for 24 h and then filtered, and diethyl ether was allowed to passively diffuse into the methanolic solutions.

C1 *$[L_3Cu_3TbCl_2(NO_3)(H_2O)_2]$.* Orange blocky crystals, 77% yield based on $TbCl_3{\cdot}6H_2O$. ATR-IR $\bar{\nu}$: 1612, 1569, 1485, 1450, 1432, 1382, 1351, 1314, 1259, 1141, 1030, 975, 756, 718 cm^{-1}. Microanalytical data found (calcd) for **C1** (calculated for $[L_3Cu_3TbCl_2(NO_3)(H_2O)_2]$, M_r = 1161.03 g mol^{-1}) C, 37.19(37.24); H, 1.71(1.91); N, 1.22(1.21).

C2 *$[L_3Cu_3HoCl_3(H_2O)_4(MeOH)](H_2O)$.* Orange blocky crystals, 56% yield based on $HoCl_3{\cdot}6H_2O$. ATR-IR $\bar{\nu}$: 1611, 1568, 1486, 1433, 1382, 1352, 1313, 1259, 1141, 1029, 975, 755, 717 cm^{-1}. Microanalytical data found (calcd) for **C2** (calculated for $[L_3Cu_3HoCl_3(H_2O)_4MeOH]$, M_r = 1208.55 g mol^{-1}) C, 36.47(36.77); H, 2.38(2.50).

C3 *$[L_3Cu_3ErCl_3(H_2O)_{3.5}(MeOH)_{0.5}](H_2O)$.* Orange platelike crystals, 84% yield based on $ErCl_3{\cdot}6H_2O$. ATR-IR $\bar{\nu}$: 1612, 1567, 1484, 1428, 1381, 3152, 1310, 1264, 1143, 1027, 981, 756, 710 cm^{-1}. Microanalytical data found (calcd) for **C3** (calculated for $[L_3Cu_3ErCl_3(H_2O)_{4.5}MeOH_{0.5}]$, M_r = 1203.87 g mol^{-1}) C, 36.70(36.42); H, 2.48(2.43).

C4 *$[L_3Cu_3Gd(NO_3)_2(H_2O)_2(MeOH)](NO_3)$.* Orange platelike crystals, 88% yield based on $Gd(NO_3)_3{\cdot}6H_2O$. ATR-IR $\bar{\nu}$: 1616, 1566, 1485, 1429, 1382, 1351, 1314, 1258, 1140, 1029, 975, 756, 718 cm^{-1}. Microanalytical data found (calcd) for **C4** (calculated for $[L_3Cu_3Gd(NO_3)_3(H_2O)_2MeOH]$, M_r = 1244.50 g mol^{-1}) C, 36.07(35.71); H, 1.97(2.11); N, 3.59(3.38).

C5 *$[L_3Cu_3Dy(NO_3)_2(H2O)_2(MeOH)](NO_3)$.* Orange platelike crystals, 47% yield based on $Dy(NO_3)_3{\cdot}6H_2O$. ATR-IR $\bar{\nu}$: 1611, 1568, 1486, 1432, 1382, 1351, 1313, 1259, 1141, 1030, 974, 755, 711 cm^{-1}. Microanalytical data found (calcd) for **C5** (calculated for $[L_3Cu_3Dy(NO_3)_3(H_2O)_2MeOH]$, M_r = 1249.75 g mol^{-1}) C, 35.72(35.56); H, 1.97(2.10); N, 3.31(3.36).

C6 *$[L_3Cu_3Yb(NO_3)_2(H_2O)_2(MeOH)](NO_3)$.* Orange blocky crystals, 44% yield based on $Yb(OAc)_3{\cdot}6H_2O$. ATR-IR $\bar{\nu}$: 1610, 1567, 1488, 1434, 1383, 1355, 1316, 1260, 1143, 1032, 975, 752, 699 cm^{-1}. Microanalytical data found (calcd) for **C6**

https://doi.org/10.1021/acsomega.1c07001
ACS Omega 2022, 7, 5537−5546

(calculated for $[L_3Cu_3Yb(NO_3)_3(H_2O)_2(MeOH)]$, M_r = 1260.30 g mol^{-1}) C, 35.08(35.26); H, 1.90(2.08); N, 3.36(3.33).

C7 *$[L_3Cu_3La(NO_3)_2(H_2O)_2(MeOH)](NO_3)$*. Orange platelike crystals, 28% yield based on $La(NO_3)_3{\cdot}6H_2O$. ATR-IR $\bar{\nu}$: 1614, 1566, 1488, 1434, 1387, 1351, 1317, 1261, 1144, 1030, 975, 751, 710 cm^{-1}. Microanalytical data found (calcd) for **C7** (calculated for $[L_3Cu_3La(NO_3)_3(H_2O)_2MeOH]$, M_r = 1226.15 g mol^{-1}) C, 36.40(36.24); H, 1.80(2.14); N, 3.41(3.43).

■ ASSOCIATED CONTENT

Supporting Information

The Supporting Information is available free of charge at https://pubs.acs.org/doi/10.1021/acsomega.1c07001.

Crystal structure and refinement details, crystal packing diagrams, $\chi_m T$ vs T and M vs H plots plus simulated fits for **C4**, plots of AC susceptibility data, and modified Arrhenius plots (PDF)

Crystallographic data (ZIP)

■ AUTHOR INFORMATION

Corresponding Author

Paul G. Plieger − *School of Natural Sciences, Massey University, Palmerston North 4442, New Zealand;* orcid.org/0000-0003-4886-7677; Email: p.g.plieger@massey.ac.nz

Authors

Tyson N. Dais − *School of Natural Sciences, Massey University, Palmerston North 4442, New Zealand;* orcid.org/0000-0003-0781-996X

Rina Takano − *Department of Engineering Science, Graduate School of Informatics and Engineering, The University of Electro-Communications, Chofu, Tokyo 182-8585, Japan*

Yoshiki Yamaguchi − *Department of Engineering Science, Graduate School of Informatics and Engineering, The University of Electro-Communications, Chofu, Tokyo 182-8585, Japan*

Takayuki Ishida − *Department of Engineering Science, Graduate School of Informatics and Engineering, The University of Electro-Communications, Chofu, Tokyo 182-8585, Japan;* orcid.org/0000-0001-9088-2526

Complete contact information is available at: https://pubs.acs.org/10.1021/acsomega.1c07001

Author Contributions

Synthesis, structural characterization, and initial draft were completed by T.N.D. and P.G.P. Magnetic characterization was completed by R.T., Y.Y., and T.I. All authors have given approval to the final version of the manuscript.

Notes

The authors declare no competing financial interest.

■ ACKNOWLEDGMENTS

T.N.D. and P.G.P. would like to thank the Massey University for the award of a Massey University Doctoral Scholarship for Māori to T.N.D. T.I. is grateful to the support from JSPS KAKENHI (JP20K21170 and JP17H06371).

■ REFERENCES

(1) Sessoli, R.; Gatteschi, D.; Caneschi, A.; Novak, M. A. Magnetic Bistability in a Metal-Ion Cluster. *Nature* **1993**, *365*, 141−143.

(2) Wernsdorfer, W.; Sessoli, R. Quantum Phase Interference and Parity Effects in Magnetic Molecular Clusters. *Science* **1999**, *284*, 133−135.

(3) Leuenberger, M. N.; Loss, D. Quantum Computing in Molecular Magnets. *Nature* **2001**, *410*, 789−793.

(4) Gatteschi, D.; Sessoli, R. Quantum Tunneling of Magnetization and Related Phenomena in Molecular Materials. *Angew. Chem., Int. Ed.* **2003**, *42*, 268−297.

(5) Hill, S.; Edwards, R. S.; Aliaga-Alcalde, N.; Christou, G. Quantum Coherence in an Exchange-Coupled Dimer of Single-Molecule Magnets. *Science* **2003**, *302*, 1015−1018.

(6) Mannini, M.; Pineider, F.; Sainctavit, P.; Danieli, C.; Otero, E.; Sciancalepore, C.; Talarico, A. M.; Arrio, M.-A.; Cornia, A.; Gatteschi, D.; Sessoli, R. Magnetic Memory of a Single-Molecule Quantum Magnet Wired to a Gold Surface. *Nat. Mater.* **2009**, *8*, 194−197.

(7) Bogani, L.; Wernsdorfer, W. Molecular Spintronics Using Single-Molecule Magnets. In *Nanoscience and Technology: A collection of reviews from Nature journals*; World Scientific, 2010; pp 194−201.

(8) Mannini, M.; Pineider, F.; Danieli, C.; Totti, F.; Sorace, L.; Sainctavit, P.; Arrio, M.-A.; Otero, E.; Joly, L.; Cezar, J. C.; Cornia, A.; Sessoli, R. Quantum Tunnelling of the Magnetization in a Monolayer of Oriented Single-Molecule Magnets. *Nature* **2010**, *468*, 417−421.

(9) Aravena, D.; Ruiz, E. Spin Dynamics in Single-Molecule Magnets and Molecular Qubits. *Dalton Trans.* **2020**, *49*, 9916−9928.

(10) Marin, R.; Brunet, G.; Murugesu, M. Shining New Light on Multifunctional Lanthanide Single-Molecule Magnets. *Angew. Chem., Int. Ed.* **2021**, *60*, 1728−1746.

(11) Gatteschi, D.; Sessoli, R.; Villain, J. *Molecular Nanomagnets*; Oxford University Press on Demand, 2006; Vol. *5*.

(12) Ishikawa, N.; Sugita, M.; Ishikawa, T.; Koshihara, S.-y.; Kaizu, Y. Lanthanide Double-Decker Complexes Functioning as Magnets at the Single-Molecular Level. *J. Am. Chem. Soc.* **2003**, *125*, 8694−8695.

(13) Chen, Y.-C.; Huang, X.-S.; Liu, J.-L.; Tong, M.-L. Magnetic Dynamics of a Neodymium(III) Single-Ion Magnet. *Inorg. Chem.* **2018**, *57*, 11782−11787.

(14) Kajiwara, T.; Nakano, M.; Takahashi, K.; Takaishi, S.; Yamashita, M. Structural Design of Easy-Axis Magnetic Anisotropy and Determination of Anisotropic Parameters of LnIII−CuII Single-Molecule Magnets. *Chem.—Eur. J.* **2011**, *17*, 196−205.

(15) Upadhyay, A.; Das, C.; Vaidya, S.; Singh, S. K.; Gupta, T.; Mondol, R.; Langley, S. K.; Murray, K. S.; Rajaraman, G.; Shanmugam, M. Role of the Diamagnetic Zinc(II) Ion in Determining the Electronic Structure of Lanthanide Single-Ion Magnets. *Chem.—Eur. J.* **2017**, *23*, 4903−4916.

(16) Gupta, S. K.; Murugavel, R. Enriching Lanthanide Single-Ion Magnetism through Symmetry and Axiality. *Chem. Commun.* **2018**, *54*, 3685−3696.

(17) Andruh, M.; Costes, J.-P.; Diaz, C.; Gao, S. 3d−4f Combined Chemistry: Synthetic Strategies and Magnetic Properties. *Inorg. Chem.* **2009**, *48*, 3342−3359.

(18) Wang, H.-L.; Zhu, Z.-H.; Peng, J.-M.; Zou, H.-H. Heterometallic 3d/4f-Metal Complexes: Structure and Magnetism. *J. Cluster Sci.* **2021**, DOI: 10.1007/s10876-021-02084-7.

(19) Liu, K.; Shi, W.; Cheng, P. Toward heterometallic single-molecule magnets: Synthetic strategy, structures and properties of 3d-4f discrete complexes. *Coord. Chem. Rev.* **2015**, *289-290*, 74−122.

(20) Sharples, J. W.; Collison, D. The coordination chemistry and magnetism of some 3d-4f and 4f amino-polyalcohol compounds. *Coord. Chem. Rev.* **2014**, *260*, 1−20.

(21) Thompson, L. K.; Dawe, L. N. Magnetic Properties of Transition Metal (Mn (II), Mn (III), Ni (II), Cu (II)) and Lanthanide (Gd (III), Dy (III), Tb (III), Eu (III), Ho (III), Yb (III)) Clusters and [Nxn] Grids: Isotropic Exchange and SMM Behaviour. *Coord. Chem. Rev.* **2015**, *289-290*, 13−31.

(22) Akine, S.; Sunaga, S.; Taniguchi, T.; Miyazaki, H.; Nabeshima, T. Core/Shell Oligometallic Template Synthesis of Macrocyclic Hexaoxime. *Inorg. Chem.* **2007**, *46*, 2959−2961.

(23) Akine, S.; Sunaga, S.; Nabeshima, T. Multistep Oligometal Complexation of the Macrocyclic Tris(N2O2) Hexaoxime Ligand. *Chem.—Eur. J.* **2011**, *17*, 6853−6861.
(24) Feltham, H. L. C.; Clérac, R.; Powell, A. K.; Brooker, S. A Tetranuclear, Macrocyclic 3d−4f Complex Showing Single-Molecule Magnet Behavior. *Inorg. Chem.* **2011**, *50*, 4232−4234.
(25) Feltham, H. L. C.; Klöwer, F.; Cameron, S. A.; Larsen, D. S.; Lan, Y.; Tropiano, M.; Faulkner, S.; Powell, A. K.; Brooker, S. A Family of 13 Tetranuclear Zinc(II)-Lanthanide(III) Complexes of a [3 + 3] Schiff-Base Macrocycle Derived from 1,4-Diformyl-2,3-Dihydroxybenzene. *Dalton Trans.* **2011**, *40*, 11425−11432.
(26) Yamashita, A.; Watanabe, A.; Akine, S.; Nabeshima, T.; Nakano, M.; Yamamura, T.; Kajiwara, T. Wheel-Shaped ErIIIZnII3 Single-Molecule Magnet: A Macrocyclic Approach to Designing Magnetic Anisotropy. *Angew. Chem.* **2011**, *50*, 4016−4019.
(27) Dais, T. N.; Brown, M. J.; Coles, M. P.; Laur, F.; Price, J. R.; Rowlands, G. J.; Plieger, P. G. Synthesis and Characterization of Co(II) and Mn(II) [M_3L3] Triangles. *J. Inclusion Phenom. Macrocyclic Chem.* **2019**, *94*, 175−182.
(28) De Silva, D. N. T.; Dais, T. N.; Jameson, G. B.; Cutler, D. J.; Brechin, E. K.; Davies, C. G.; Jameson, G. N. L.; Plieger, P. G. Synthesis and Characterization of Symmetrically versus Unsymmetrically Proton-Bridged Hexa-Iron Clusters. *ACS Omega* **2021**, *6*, 16661.
(29) Woodhouse, S. S.; Buchanan, J. K.; Dais, T. N.; Ainscough, E. W.; Brodie, A. M.; Freeman, G. H.; Plieger, P. G. Structural Trends in a Series of Bulky Dialkylbiarylphosphane Complexes of CuI. *Acta Crystallogr., Sect. C: Struct. Chem.* **2021**, *77*, 513.
(30) Dais, T. N.; Takano, R.; Ishida, T.; Plieger, P. G. Self-Assembly of Non-Macrocyclic Triangular Ni3Ln Clusters. *Dalton Trans* **2021**, *51*, 1446.
(31) Maity, S.; Bhunia, P.; Ichihashi, K.; Ishida, T.; Ghosh, A. SMM Behaviour of Heterometallic Dinuclear CuIILnIII (Ln = Tb and Dy) Complexes Derived from N2O3 Donor Unsymmetrical Ligands. *New J. Chem.* **2020**, *44*, 6197−6205.
(32) Mahapatra, P.; Koizumi, N.; Kanetomo, T.; Ishida, T.; Ghosh, A. A Series of CuII−LnIII Complexes of an N2O3 Donor Asymmetric Ligand and a Possible CuII−TbIII SMM Candidate in No Bias Field. *New J. Chem.* **2019**, *43*, 634−643.
(33) Ueno, T.; Fujinami, T.; Matsumoto, N.; Furusawa, M.; Irie, R.; Re, N.; Kanetomo, T.; Ishida, T.; Sunatsuki, Y. Circular and Chainlike Copper(II)−Lanthanide(III) Complexes Generated by Assembly Reactions of Racemic and Chiral Copper(II) Cross-Linking Ligand Complexes with LnIII(NO3)3·6H2O (LnIII = GdIII, TbIII, DyIII). *Inorg. Chem.* **2017**, *56*, 1679−1695.
(34) Mahapatra, P.; Ghosh, S.; Koizumi, N.; Kanetomo, T.; Ishida, T.; Drew, M. G. B.; Ghosh, A. Structural Variations in (CuL)2Ln Complexes of a Series of Lanthanide Ions with a Salen-Type Unsymmetrical Schiff Base (H2L): Dy and Tb Derivatives as Potential Single-Molecule Magnets. *Dalton Trans.* **2017**, *46*, 12095−12105.
(35) Ghosh, S.; Mahapatra, P.; Kanetomo, T.; Drew, M. G. B.; Ishida, T.; Ghosh, A. Syntheses, Crystal Structure and Magnetic Properties of an Unprecedented One-Dimensional Coordination Polymer Derived from an {(NiL)2Ln} Node and a Pyrazine Spacer (H2L = N,N′-Bis(Salicylidene)-1,3-Propanediamine, Ln = Gd, Tb and Dy). *ChemistrySelect* **2016**, *1*, 2722−2729.
(36) Dhers, S.; Feltham, H. L. C.; Clérac, R.; Brooker, S. Design of One-Dimensional Coordination Networks from a Macrocyclic {3d-4f} Single-Molecule Magnet Precursor Linked by [W(CN)8]3- Anions. *Inorg. Chem.* **2013**, *52*, 13685−13691.
(37) Dhers, S.; Feltham, H. L. C.; Rouzières, M.; Clérac, R.; Brooker, S. Macrocyclic {3d-4f} SMMs as Building Blocks for 1D-Polymers: Selective Bridging of 4f Ions by Use of an O-Donor Ligand. *Dalton Trans.* **2016**, *45*, 18089−18093.
(38) Dhers, S.; Feltham, H. L. C.; Rouzières, M.; Clérac, R.; Brooker, S. Discrete versus Chain Assembly: Hexacyanometallate Linkers and Macrocyclic {3d-4f} Single-Molecule Magnet Building Blocks. *Inorg. Chem.* **2019**, *58*, 5543−5554.
(39) Feltham, H. L. C.; Clérac, R.; Ungur, L.; Vieru, V.; Chibotaru, L. F.; Powell, A. K.; Brooker, S. Synthesis and Magnetic Properties of a New Family of Macrocyclic MII3LnIII Complexes: Insights into the Effect of Subtle Chemical Modification on Single-Molecule Magnet Behavior. *Inorg. Chem.* **2012**, *51*, 10603−10612.
(40) Feltham, H. L. C.; Dhers, S.; Rouzières, M.; Clérac, R.; Powell, A. K.; Brooker, S. A Family of Fourteen Soluble Stable Macrocyclic [NiII3LnIII] Heterometallic 3d-4f Complexes. *Inorg. Chem. Front.* **2015**, *2*, 982−990.
(41) Feltham, H. L. C.; Lan, Y.; Klöwer, F.; Ungur, L.; Chibotaru, L. F.; Powell, A. K.; Brooker, S. A Non-Sandwiched Macrocyclic Monolanthanide Single-Molecule Magnet: The Key Role of Axiality. *Chem.—Eur. J.* **2011**, *17*, 4362−4365.
(42) Dey, A.; Bag, P.; Kalita, P.; Chandrasekhar, V. Heterometallic CuII−LnIII Complexes: Single Molecule Magnets and Magnetic Refrigerants. *Coord. Chem. Rev.* **2021**, *432*, 213707.
(43) Tang, J.-K.; Wang, Q.-L.; Si, S.-F.; Liao, D.-Z.; Jiang, Z.-H.; Yan, S.-P.; Cheng, P. A Novel Tetranuclear Lanthanide(III)−Copper(II) Complex of the Macrocyclic Oxamide [PrCu3] (Macrocyclic Oxamide=1,4,8,11-Tetraazacyclotradecanne-2,3-Dione): Synthesis, Structure and Magnetism. *Inorg. Chim. Acta* **2005**, *358*, 325−330.
(44) Kettles, F. J.; Milway, V. A.; Tuna, F.; Valiente, R.; Thomas, L. H.; Wernsdorfer, W.; Ochsenbein, S. T.; Murrie, M. Exchange Interactions at the Origin of Slow Relaxation of the Magnetization in {TbCu3} and {DyCu3} Single-Molecule Magnets. *Inorg. Chem.* **2014**, *53*, 8970−8978.
(45) Worrell, A.; Sun, D.; Mayans, J.; Lampropoulos, C.; Escuer, A.; Stamatatos, T. C. Oximato-Based Ligands in 3d/4f-Metal Cluster Chemistry: A Family of {Cu3Ln} Complexes with a "Propeller"-like Topology and Single-Molecule Magnetic Behavior. *Inorg. Chem.* **2018**, *57*, 13944−13952.
(46) Pinsky, M.; Avnir, D. Continuous Symmetry Measures. 5. The Classical Polyhedra. *Inorg. Chem.* **1998**, *37*, 5575−5582.
(47) Casanova, D.; Cirera, J.; Llunell, M.; Alemany, P.; Avnir, D.; Alvarez, S. Minimal Distortion Pathways in Polyhedral Rearrangements. *J. Am. Chem. Soc.* **2004**, *126*, 1755−1763.
(48) Borrás-Almenar, J. J.; Clemente-Juan, J. M.; Coronado, E.; Tsukerblat, B. S. High-Nuclearity Magnetic Clusters: Generalized Spin Hamiltonian and Its Use for the Calculation of the Energy Levels, Bulk Magnetic Properties, and Inelastic Neutron Scattering Spectra. *Inorg. Chem.* **1999**, *38*, 6081−6088.
(49) Borrás-Almenar, J.; Clemente-Juan, J. M.; Coronado, E.; Tsukerblat, B. S. MAGPACK 1 A Package to Calculate the Energy Levels, Bulk Magnetic Properties, and Inelastic Neutron Scattering Spectra of High Nuclearity Spin Clusters. *J. Comput. Chem.* **2001**, *22*, 985−991.
(50) Bartolomé, J.; Filoti, G.; Kuncser, V.; Schinteie, G.; Mereacre, V.; Anson, C. E.; Powell, A. K.; Prodius, D.; Turta, C. Magneto-structural Correlations in the Tetranuclear Series of Fe3LnO2 Butterfly Core Clusters: Magnetic and Mössbauer Spectroscopic Study. *Phys. Rev. B: Condens. Matter Mater. Phys.* **2009**, *80*, 014430.
(51) Sessoli, R.; Powell, A. K. Strategies towards Single Molecule Magnets Based on Lanthanide Ions. *Coord. Chem. Rev.* **2009**, *253*, 2328−2341.
(52) Cole, K. S.; Cole, R. H. Dispersion and Absorption in Dielectrics I. Alternating Current Characteristics. *J. Chem. Phys.* **1941**, *9*, 341−351.
(53) Andruh, M.; Ramade, I.; Codjovi, E.; Guillou, O.; Kahn, O.; Trombe, J. C. Crystal Structure and Magnetic Properties of [Ln2Cu4] Hexanuclear Clusters (Where Ln = Trivalent Lanthanide). Mechanism of the Gadolinium(III)-Copper(II) Magnetic Interaction. *J. Am. Chem. Soc.* **1993**, *115*, 1822−1829.
(54) Costes, J.-P.; Dahan, F.; Dupuis, A.; Laurent, J.-P. Is Ferromagnetism an Intrinsic Property of the CuII/GdIII Couple? 1. Structures and Magnetic Properties of Two Novel Dinuclear Complexes with a μ-Phenolato−μ-Oximato (Cu,Gd) Core. *Inorg. Chem.* **2000**, *39*, 169−173.

https://doi.org/10.1021/acsomega.1c07001
ACS Omega 2022, 7, 5537−5546

(55) Shimada, T.; Okazawa, A.; Kojima, N.; Yoshii, S.; Nojiri, H.; Ishida, T. Ferromagnetic Exchange Couplings Showing a Chemical Trend in Cu−Ln−Cu Complexes (Ln = Gd, Tb, Dy, Ho, Er). *Inorg. Chem.* **2011**, *50*, 10555−10557.
(56) Watanabe, R.; Fujiwara, K.; Okazawa, A.; Tanaka, G.; Yoshii, S.; Nojiri, H.; Ishida, T. Chemical Trend of Ln−M Exchange Couplings in Heterometallic Complexes with Ln = Gd, Tb, Dy, Ho, Er and M = Cu, V. *Chem. Commun.* **2011**, *47*, 2110−2112.
(57) Feltham, H. L. C.; Clérac, R.; Ungur, L.; Chibotaru, L. F.; Powell, A. K.; Brooker, S. By Design: A Macrocyclic 3d-4f Single-Molecule Magnet with Quantifiable Zero-Field Slow Relaxation of Magnetization. *Inorg. Chem.* **2013**, *52*, 3236−3240.
(58) Ishida, T. *Spin-Parity Behavior in the Exchange-Coupled Lanthanoid-Nitroxide Molecular Magnets*; IOP Publishing, 2017; Vol. *202*, p 012001.
(59) Kanetomo, T.; Kihara, T.; Miyake, A.; Matsuo, A.; Tokunaga, M.; Kindo, K.; Nojiri, H.; Ishida, T. Giant Exchange Coupling Evidenced with a Magnetization Jump at 52 T for a Gadolinium-Nitroxide Chelate. *Inorg. Chem.* **2017**, *56*, 3310−3314.
(60) Mehr, S. H. M.; Depmeier, H.; Fukuyama, K.; Maghami, M.; MacLachlan, M. J. Formylation of Phenols Using Formamidine Acetate. *Org. Biomol. Chem.* **2017**, *15*, 581−583.
(61) Bruker, A. X. S.*APEX3, SADABS and SAINT*; Bruker AXS Inc: Madison, Wisconsin, USA, 2016.
(62) Sheldrick, G. M. SHELXT- Integrated space-group and crystal-structure determination. *Acta Crystallogr.* **2015**, *71*, 3−8.
(63) Sheldrick, G. M. Crystal structure refinement withSHELXL. *Acta Crystallogr., Sect. C: Struct. Chem.* **2015**, *71*, 3−8.
(64) Dolomanov, O. V.; Bourhis, L. J.; Gildea, R. J.; Howard, J. A. K.; Puschmann, H. OLEX2: A Complete Structure Solution, Refinement and Analysis Program. *J. Appl. Crystallogr.* **2009**, *42*, 339−341.

https://doi.org/10.1021/acsomega.1c07001
ACS Omega 2022, 7, 5537−5546